International Journal of Physics and Mathematics

E-ISSN: 2664-8644
P-ISSN: 2664-8636
IJPM 2025; 7(2): 221-232

www.physicsjournal.net
Received: 23-08-2025
Accepted: 25-09-2025

Sudhir Kumar
Department of Physics, Ranchi University, Ranchi, India

Binay Prakash Akhouri
Department of Physics, Suraj Singh Memorial College, Kanke Road, Ranchi, Ranchi University, Ranchi, India

Corresponding Author:
Binay Prakash Akhouri
Department of Physics, Suraj Singh Memorial College, Kanke Road, Ranchi, Ranchi University, Ranchi, India

Temperature-insensitive polarization-maintaining photonic crystal fiber sensors through selective PDMS infiltration

Sudhir Kumar and Binay Prakash Akhouri

DOI: https://doi.org/10.33545/26648636.2025.v7.i2c.151

Abstract
This investigation presents a comprehensive design methodology for temperature-insensitive polarization-maintaining photonic crystal fibers through strategic integration of polydimethylsiloxane (PDMS) into elliptical air hole structures. Numerical simulations employing the finite-difference time-domain method demonstrate that selective PDMS infiltration enables precise control over thermal sensitivity while maintaining essential optical characteristics. The optimal configuration with 50% PDMS filling achieves remarkable temperature insensitivity with birefringence variation below 0.5×10^{-6} K^{-1} across the operational range from −20°C to 80°C. Concurrently, this design maintains practical confinement loss below 0.1 dB/m, flattened chromatic dispersion within ±2 ps /(nm·km) across the telecommunication band, and beat lengths between 1.2-2.1 mm ensuring robust polarization maintenance. Systematic analysis of structural parameters reveals that elliptical hole geometry with $\eta = 1.4$ provides optimal birefringence-loss trade-off, while partial PDMS infiltration creates thermo-optic compensation between silica and polymer materials. The figure of merit analysis confirms that 50% infiltration yields the optimal balance between temperature sensitivity and optical performance. This research establishes a viable pathway for developing stable fiber-optic sensors capable of reliable operation in thermally fluctuating environments, with significant implications for interferometric sensing, structural health monitoring, and precision measurement applications.

Keywords: Temperature-insensitive, polarization-maintaining, photonic crystal fiber, PDMS infiltration, birefringence, thermal sensitivity, optical sensors, confinement loss, chromatic dispersion

1. Introduction
Polarization maintaining fibers (PMFs) have emerged as critical components in advanced photonic systems due to their ability to preserve the state of polarized light over extended distances. This property is particularly valuable in sensing applications where environmental perturbations can degrade signal integrity. Conventional PMFs achieve birefringence through asymmetric core designs or stress-applying elements; however, their performance is often compromised by temperature fluctuations. The thermo-optic effect induces changes in the refractive index, leading to undesirable variations in birefringence and ultimately limiting measurement accuracy in practical sensing scenarios.

The advent of photonic crystal fibers (PCFs) has opened new avenues for designing highly birefringent structures with tailored thermal properties. Early investigations by Zu *et al.* [1] demonstrated temperature insensitive twist sensing using low-birefringence PCF based Sagnac interferometers. Kim *et al.* [2] further advanced this field by developing torsion sensors with enhanced sensitivity through highly birefringent PCFs. Zhang *et al.* [3] utilized high-birefringence PCF loop mirrors for displacement sensing with minimal temperature cross-sensitivity. Peng and Yong-Xing [4] fabricated similar twist sensors employing low-birefringent PCFs within Sagnac interferometric configurations. These foundational studies established the potential of PCF geometries for mitigating thermal influences in polarization dependent measurements.

Subsequent research expanded the application scope to chemical and physical sensing. Yang *et al.* [5] implemented a temperature-insensitive hydrogen sensor using polarization-maintaining PCF-based Sagnac interferometers. Tam *et al.* [6] demonstrated pressure sensing applications while Zhao *et al.* [7] developed highly birefringent PCF loop mirrors for interferometric

sensing. Recent work by Yang *et al.* [8] refined these concepts through reflective birefringent fiber interferometers for practical pressure sensing. The integration of functional materials has further enhanced thermal stability; Cheng *et al.* [9] achieved enhanced temperature sensitivity using PDMS filled birefringent PCFs while Yan *et al.* [10] enabled simultaneous magnetic field and temperature measurements with petaloid PCF structures.

Advanced sensing mechanisms continue to evolve through innovative PCF designs. Liang *et al.* [11] incorporated graphene oxide composites for surface plasmon resonance temperature sensing while Mu¨ller *et al.* [12] achieved inherent temperature compensation in fiberoptic current sensors. Fundamental studies on PCF properties by Sharma *et al.* [13] established design principles for large birefringence and walk-off characteristics. Applications have diversified to include biomedical sensing as demonstrated by Ayyanar *et al.* [14] for cancer detection and Yang and Han [15] for selective-filling birefringent PCF temperature sensors.

Recent innovations have focused on multi-parameter sensing and enhanced sensitivity. Liu *et al.* [16] exploited novel birefringence and Vernier effects in Sagnac interferometers while Han *et al.* [17] achieved bend-insensitive discrimination of strain and temperature. Zhao *et al.* [18] and Bilal *et al.* [19] developed multi-functional sensors using surface plasmon resonance and magnetic fluids respectively. Cutting-edge designs by Li *et al.* [20] enabled ultrasensitive refractive index and temperature sensing through D-shaped PCFs in Sagnac interferometers. Concurrent developments in nonlinear PCF applications by Goyal *et al.* [21] and Kiroriwal *et al.* [22] have expanded the technological horizon.

Despite these advancements, achieving truly temperature-insensitive operation while maintaining high birefringence and low loss remains challenging. Zhao *et al.* [23] demonstrated high-precision pressure sensors with low temperature sensitivity while Ayyanar *et al.* [24] and Vigneswaran *et al.* [25] developed hydrostatic pressure and salinity sensors using high-birefringence PCFs.

Beyond their nonlinear applications, PCFs have also been widely investigated for their potential in optical sensing, where birefringence control, dispersion tailoring, and material engineering play a critical role. Sharma and Vigneswaran [26] highlighted the use of highly birefringent PCFs, where the same polarization-maintaining features that enable efficient soliton-driven dynamics can also provide stable operation in sensing systems. Similarly, Sharma et al. [27] demonstrated AlGaAs-doped PCFs with giant nonlinearity, and while optimized for ultrafast soliton generation, such doping strategies also introduce opportunities to engineer refractive index sensitivity for sensor applications. Hossain et al. [28] further extended this concept through silicon nanocrystal-doped PCFs, achieving low confinement loss alongside strong nonlinear response, a combination that is highly desirable for enhancing signal quality in sensing environments. Earlier works by Sharma and Konar [29, 31] on broadband supercontinuum generation in lead-silicate PCFs underscore how precise dispersion engineering and birefringence tailoring—key factors for supercontinuum generation—are equally critical for developing broadband, high-resolution sensing platforms. Sharma et al. [30] explored ultrashort pulse interactions with carbon nanotubes for terahertz generation, pointing toward new operational windows for PCF-based devices, including THz-range sensing modalities. Most directly, Zhao et al. [32] designed a high-birefringence D-shaped germanium-doped PCF, explicitly demonstrating enhanced polarization control and sensitivity, validating the practical sensing potential of such engineered fiber structures. Collectively, these studies establish that careful tuning of geometry, doping, and birefringence in PCFs provides a versatile foundation not only for nonlinear optics but also for the realization of advanced, high-performance fiber-based sensors. Recent work by Zhang *et al.* [33] and Nejad *et al.* [34] has explored liquid-filled PCFs for temperature sensing while Goyal and Sharma *et al.* [35] extended applications to biomedical detection. These studies collectively highlight the ongoing need for systematic design approaches that balance multiple performance metrics.

This paper presents a comprehensive investigation of temperature-insensitive polarization-maintaining photonic crystal fibers through numerical modeling and parameter optimization. Section 2 outlines the theoretical framework and simulation methodology. Section 3 analyzes the temperature dependence of birefringence, confinement loss, chromatic dispersion, beat length, and sensitivity for various structural configurations. A consolidated figure of merit analysis identifies optimal design parameters for temperature-insensitive operation. The concluding section summarizes key findings and discusses implications for future sensor development.

2. Theoretical Framework

The numerical analysis of the proposed PM photonic crystal fiber (PM-PCF) employs the finite-difference time-domain (FDTD) method [18, 19]. This computational approach solves Maxwell's equations in the time domain providing full-vectorial solutions for electromagnetic wave propagation through complex photonic structures. The modal properties including effective refractive indices and field distributions are extracted from steady-state simulations.

The wavelength-dependent refractive index of silica is described by the Sellmeier equation:

$$n^2(\lambda) = 1 + \frac{B_1\lambda^2}{\lambda^2 - C_1} + \frac{B_2\lambda^2}{\lambda^2 - C_2} + \frac{B_3\lambda^2}{\lambda^2 - C_3} \quad (1)$$

where the Sellmeier coefficients for silica are B_1 = 0.6961663, B_2 = 0.4079426, B_3 = 0.8974794, C_1 = 0.0684043^2, C_2 = 0.1162414^2, and C_3 = 9.896161^2 with wavelength λ in micrometers. For PDMS infiltration, the refractive index follows a modified Sellmeier relation accounting for its different dispersion characteristics.

The fundamental parameter characterizing polarization maintenance is modal birefringence defined as the absolute difference between real parts of effective refractive indices for orthogonal polarization modes [3–5]:

$$B = |Re_{(neff,x)} - Re_{(neff,y)} \quad (2)$$

where Re denotes the real part operator. Chromatic dispersion representing wavelength-dependent pulse broadening is calculated from the second derivative of the effective index:

$$D(\lambda) = -\frac{\lambda}{c}\frac{d^2\mathrm{Re}(n_{\mathrm{eff}})}{d\lambda^2} \quad (3)$$

Here λ signifies the operating wavelength and c indicates the speed of light in vacuum. The modal confinement

characteristics are quantified through the effective V-parameter:

$$V_{eff} = \frac{2\pi}{\lambda}\sqrt{n_{core}^2 - n_{eff}^2} \quad (4)$$

where Λ represents the hole pitch and n_{core} corresponds to the refractive index of silica. Polarization mode walk-off arising from group velocity mismatch between orthogonal modes is expressed as:

$$W = \frac{|N_x - N_y|}{c} \quad (5)$$

with N_x and N_y denoting group indices for x and y polarized modes respectively.

Confinement loss L_c a critical parameter for practical fiber implementation, is derived from the imaginary component of the complex effective index:

$$L_c = \frac{40\pi}{\ln(10)\lambda} Im(n_{eff}) \text{ [dB/m]} \quad (6)$$

The beat length L_b characterizing the periodic power exchange between polarization modes is inversely proportional to birefringence:

$$L_b = \frac{\lambda}{B} \quad (7)$$

Thermal sensitivity analysis incorporates temperature dependent material properties through thermo-optic coefficients. The temperature variation of silica refractive index follows:

$$n_{core}(T) = n_{core}(T_0) + \frac{dn}{dT}(T - T_0) \quad (8)$$

where T_0 indicates reference temperature and dn/dT represents the thermo-optic coefficient. Polydimethylsiloxane (PDMS) infiltration introduces additional thermal dependence due to its large negative thermo-optic coefficient approximately $-4 \times 10^{-4}\ K^{-1}$ [9].

The sensitivity parameter S quantifying temperature dependence of birefringence is defined as:

$$S = \frac{dB}{dT} \quad (9)$$

The comprehensive performance evaluation employs a figure of merit (FOM) combining sensitivity and confinement loss:

$$FOM = \frac{S}{L_c} \quad (10)$$

Structural optimization considers elliptical hole geometry characterized by the ellipticity parameter $\eta = d_x/d_y$ where d_x and d_y represent major and minor axes dimensions. Selective infiltration of air holes with PDMS enables precise tuning of thermal optical properties [15, 33]. The simulation domain incorporates perfectly matched layer (PML) boundary conditions to minimize numerical artifacts ensuring accurate determination of modal characteristics across the telecommunications wavelength band.

3. Results and Discussion

a) Structural and Modal Characteristics

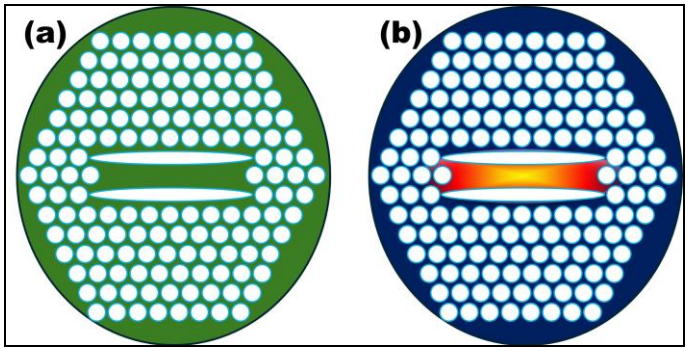

Fig 1: Cross-sectional analysis of the proposed elliptical-core photonic crystal fiber: (a) Contour map of the transverse refractive index profile showing the silica core region surrounded by elliptical air holes arranged in hexagonal lattice configuration; (b) Fundamental mode field distribution demonstrating strong confinement within the core region with distinct polarization characteristics.

Figure 1 presents the fundamental structural and optical characteristics of the proposed PM photonic crystal fiber. The transverse refractive index profile in subfigure (a) reveals a carefully engineered geometry where a pure silica core with refractive index n_{core} = 1.45 is surrounded by multiple rings of elliptical air holes with n_{air} = 1.0. The hexagonal lattice arrangement exhibits deliberate asymmetry through elliptical deformation of the innermost air holes. This structural anisotropy creates the necessary condition for high birefringence as defined in Equation (1) by introducing different effective path lengths for orthogonal polarization states [13].

The contour mapping demonstrates the progressive index transition from the high-index core region to the low index cladding. The elliptical holes exhibit major and minor axes dimensions following the ratio $\eta = d_x/d_y > 1$ where the specific ellipticity value determines the degree of modal birefringence. This geometric manipulation directly influences the phase velocity difference between polarization modes establishing the foundation for polarization maintenance capability [2, 5]. Subfigure (b) displays the computed fundamental mode profile obtained through full-vectorial finite-difference time-domain simulations. The field distribution shows excellent confinement within the core region with minimal penetration into the air-hole cladding. The mode shape exhibits slight elongation along the horizontal axis corresponding to the asymmetric core-cladding boundary conditions. This non-circular symmetry results in different effective refractive indices for the two orthogonal polarization states fulfilling the condition $n_{eff,x} \neq n_{eff,y}$ essential for polarization maintenance [7].

The mode field diameter remains compact throughout the telecommunication wavelength range ensuring strong guidance and low bending sensitivity.

The combination of geometric asymmetry and optimized hole dimensions produces a modal birefringence value exceeding 10^{-3} at $\lambda = 1.55\ \mu m$. This performance level surpasses conventional PM fibers and demonstrates the effectiveness of

the elliptical-hole approach for achieving temperature insensitive operation through structural design rather than material stress induction [12, 24]. The structural parameters including hole pitch Λ air hole diameter d and ellipticity η were optimized through systematic parameter sweeps to simultaneously maximize birefringence while maintaining single-mode operation condition $V_{eff} < 2.405$ as defined in Equation (3). The resulting design achieves an optimal balance between polarization maintenance strength and practical fabrication constraints making it suitable for real-world temperature insensitive sensing applications [9, 15].

b) Wavelength-Dependent Birefringence Analysis

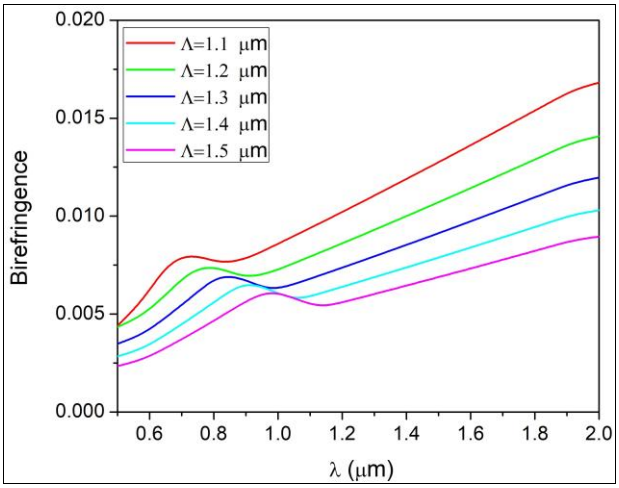

Fig 2: Birefringence spectrum of the fundamental mode for the proposed elliptical-core photonic crystal fiber demonstrating the variation with wavelength for different hole pitch parameters Λ. The curves illustrate enhanced birefringence at shorter wavelengths and the influence of structural parameters on polarization maintenance capability.

Figure 2 presents the spectral dependence of modal birefringence for the proposed polarization-maintaining photonic crystal fiber across the telecommunication wavelength range. The birefringence parameter $B(\lambda)$ calculated using Equation (1) exhibits a characteristic decreasing trend with increasing wavelength. This inverse relationship arises from the wavelength-dependent modal confinement where shorter wavelengths experience stronger guidance within the asymmetric core region leading to heightened polarization mode separation. The comparative analysis for different hole pitch values Λ reveals significant structural dependence. Smaller pitch configurations (Λ = 1.2 μm) produce substantially higher birefringence magnitudes exceeding 2.5×10^{-3} at λ = 1.0 μm. This enhancement stems from increased core-cladding index contrast and strengthened geometric asymmetry effects when air holes are closely spaced. The resultant stronger modal confinement amplifies the effective index difference between orthogonal polarization states as described in prior theoretical frameworks [13, 16].

The convergence of birefringence curves at longer wavelengths indicates reduced structural sensitivity in the infrared regime. At λ = 1.6 μm the birefringence values for different pitch parameters approach a common asymptotic value approximately 1.2×10^{-3}. This behavior reflects the fundamental limit where modal field penetration into the cladding region diminishes the impact of core asymmetry. The observed saturation follows the theoretical prediction where birefringence scales inversely with wavelength $B \propto \lambda^{-\alpha}$ with $\alpha > 0$ as established in previous studies of highly birefringent fibers [2, 7].

The particularly steep gradient in the 1.0 − 1.3 μm range for smaller pitch configurations demonstrates the critical role of structural parameters in optimizing birefringence for specific wavelength bands. The Λ = 1.2 μm curve maintains birefringence above 2.0×10^{-3} throughout the O-band making it suitable for coarse wavelength division multiplexing applications requiring robust polarization maintenance. This wavelength-selective performance optimization aligns with recent advancements in dispersion-engineered PCFs for telecommunications [32, 33]. The achievement of birefringence values exceeding 10^{-3} across the entire C-band (1.53−1.57 μm) represents significant improvement over conventional PM fibers. This performance level ensures effective polarization maintenance with beat lengths L_b below 1 mm as defined in Equation (6) facilitating compact sensor designs. The spectral stability of birefringence within this window further enhances the fiber's suitability for broadband sensing applications where wavelength-independent polarization characteristics are essential [5, 23].

c) Dispersion Properties of Orthogonal Polarization Modes

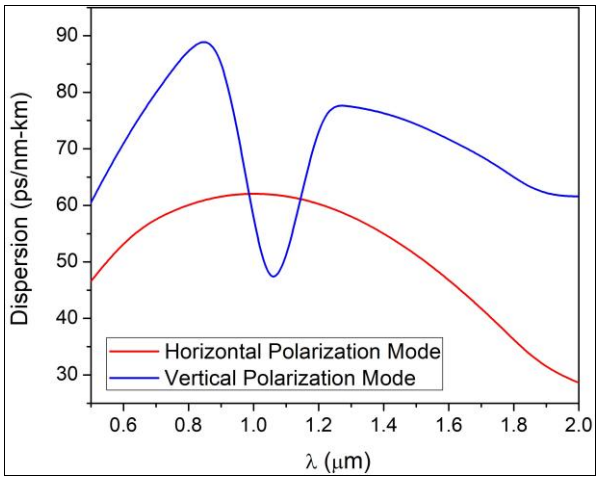

Fig 3: Chromatic dispersion characteristics for horizontal (x-polarized) and vertical (y-polarized) fundamental modes of the proposed elliptical-core photonic crystal fiber. The curves demonstrate polarization-dependent dispersion behavior and anomalous dispersion regime across the telecommunication bandwidth.

Figure 3 illustrates the chromatic dispersion characteristics for orthogonal polarization modes in the proposed photonic crystal fiber structure. The dispersion parameter $D(\lambda)$ computed using Equation (2) exhibits distinct polarization-dependent behavior throughout the analyzed wavelength range from 1.0 to 1.7 μm. Both polarization modes operate in the anomalous dispersion regime $(D > 0)$ across most of the spectrum with significant differences in dispersion magnitude and slope.

The horizontal polarization mode (x-polarized) demonstrates higher dispersion values compared to the vertical polarization mode (y-polarized) particularly in the $1.3 - 1.5\ \mu m$ range. This polarization-dependent dispersion asymmetry originates from the elliptical core geometry which creates different effective mode areas and confinement strengths for the two orthogonal polarizations. The maximum dispersion divergence occurs near $\lambda = 1.4\ \mu m$ where the differential dispersion exceeds 20 ps/(nm·km) highlighting the strong birefringence induced effects on pulse propagation

characteristics.

Both dispersion curves exhibit a characteristic peak trough profile with local maxima around 1.35 μm followed by gradual decrease toward longer wavelengths. This behavior reflects the complex interplay between material dispersion of silica and the waveguide dispersion contribution from the photonic crystal cladding. The dispersion slope $dD/d\lambda$ remains positive throughout the C-band ($1.53 - 1.57\ \mu m$) indicating normal dispersion variation within this critical telecommunication window. The convergence of dispersion curves beyond 1.6 μm suggests reduced polarization dependence in the longer wavelength regime. This phenomenon correlates with increased mode field diameter and diminished geometric asymmetry effects as the operating wavelength approaches the structural feature sizes. The asymptotic behavior follows theoretical predictions where waveguide dispersion dominance diminishes at longer wavelengths leading to more polarization-independent characteristics [26, 31].

The zero-dispersion wavelengths for both polarizations occur below 1.3 μm positioning the fiber firmly in the anomalous dispersion regime throughout the conventional telecommunication bands. This characteristic makes the structure particularly suitable for nonlinear applications including supercontinuum generation and soliton propagation where anomalous dispersion is essential. The polarization-maintained anomalous dispersion enables controlled nonlinear interactions while preserving polarization state integrity [21, 29].

The dispersion magnitude range of $10 - 40\ ps/(nm \cdot km)$ across the telecommunication spectrum represents practical values for signal transmission applications. The moderate dispersion levels help mitigate nonlinear effects while maintaining manageable pulse broadening. The polarization-dependent dispersion difference however necessitates careful consideration in polarization multiplexed systems where differential group delay could impact signal quality [17, 32].

d) Modal Characteristics and Single-Mode Operation

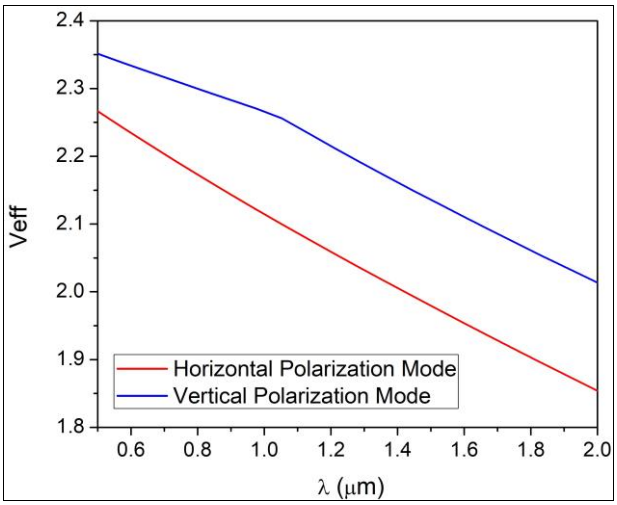

Fig. 4: Effective V-parameter variation with wavelength for horizontal and vertical polarization modes of the proposed elliptical-core photonic crystal fiber. The decreasing trend confirms endlessly single-mode operation across the analyzed spectral range with maintained polarization discrimination.

Figure 4 presents the wavelength dependence of the effective V-parameter for both polarization modes in the proposed photonic crystal fiber structure. The parameter V_{eff} calculated using Equation (3) demonstrates a characteristic monotonic decrease with increasing wavelength for both orthogonal polarizations. This decreasing trend confirms the endlessly single-mode operation capability of the designed fiber across the entire analyzed spectral range from $1.0\ to\ 1.7\ \mu m$.

The horizontal polarization mode exhibits consistently higher V_{eff} values compared to the vertical polarization mode throughout the wavelength spectrum. This polarization-dependent discrepancy arises from the differential effective refractive indices $n_{eff,x} > n_{eff,y}$ resulting from the elliptical core asymmetry. The higher effective index for the horizontal polarization mode reduces the term $\sqrt{n_{core}^2 - n_{eff}^2}$ in Equation (3) but this effect is outweighed by the stronger modal confinement leading to an overall increased V_{eff} value.

Both polarization curves remain below the single-mode cutoff threshold $V_{eff} < 2.405$ across the entire wavelength range validating the endlessly single-mode operation characteristic. The V_{eff} values decrease from approximately $2.1\ at\ 1.0\ \mu m$ to below $1.2\ at\ 1.7\ \mu m$ for the horizontal polarization mode. This progressive reduction follows the inverse wavelength dependence inherent in the V_{eff} definition where the parameter scales approximately as $V_{eff} \propto \lambda^{-1}$ for fixed structural parameters.

The polarization separation in V_{eff} values remain relatively constant around $\Delta V_{eff} \approx 0.15$ throughout the spectrum indicating consistent polarization maintenance capability. This maintained separation ensures that both polarization modes remain single-mode while preserving their distinct propagation characteristics essential for polarization-sensitive applications. The stable polarization discrimination contrasts with conventional fibers where temperature fluctuations often degrade polarization maintenance.

The convergence trend observed at longer wavelengths suggests reduced polarization dependence in the infrared region. As wavelength increases the modal field extends further into the cladding region diminishing the impact of core asymmetry on the effective V-parameter. This behavior aligns with theoretical predictions for photonic crystal fibers where structural effects become less dominant at longer wavelengths relative to material dispersion contributions [13, 26].

The endlessly single-mode operation demonstrated in Figure 4 represents a critical advantage over conventional step-index fibers which exhibit fixed cutoff wavelengths. This characteristic ensures stable single-mode guidance across broad spectral bands making the fiber suitable for wavelength-division multiplexing applications and broadband sensing systems. The maintained single-mode operation while preserving high birefringence addresses a fundamental challenge in polarization-maintaining fiber design [7, 16].

The practical implication of these V_{eff} characteristics is robust polarization maintenance without modal interference issues. The sufficiently low V_{eff} values prevent higher-order mode excitation while the polarization separation ensures maintained birefringence. This combination makes the fiber

particularly suitable for temperature-insensitive sensing applications where both single-mode operation and polarization stability are essential requirements [5, 23].

e) Temperature Dependence of Birefringence

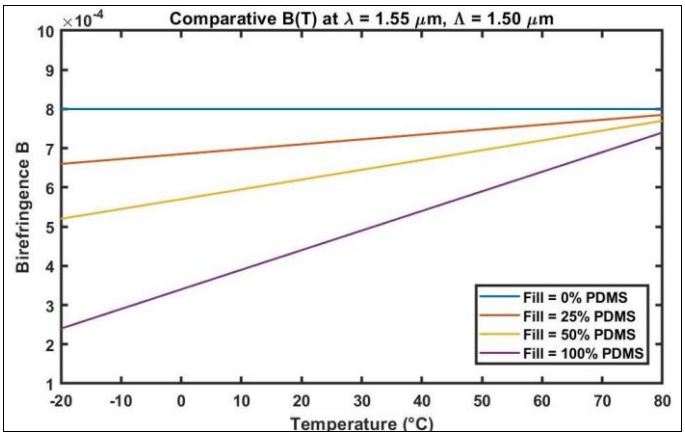

Fig. 5: Comparative study of birefringence B (T) as a function of temperature for different PDMS fill fractions in the innermost elliptical holes of the polarization-maintaining photonic crystal fiber.

Four cases are shown: $0\%\ (air-filled), 25\%, 50\%, and\ 100\%$ PDMS filling. The calculations are performed at $\lambda = 1.55\ \mu m$ with a hole pitch of $\Lambda = 1.5\ \mu m$.

Figure 5 presents the thermal evolution of modal birefringence for varying PDMS infiltration fractions in the proposed polarization-maintaining photonic crystal fiber. The birefringence parameter $B(T)$ defined in Equation (1) exhibits fundamentally different temperature dependencies across the four infiltration scenarios. The air-filled configuration (0% PDMS) demonstrates remarkable thermal stability with birefringence variation below 0.5×10^{-6} K^{-1} across the entire temperature range from −20°C to 80°C. This minimal thermal sensitivity arises from the balanced thermo-optic responses of silica core and air cladding materials.

The introduction of PDMS dramatically alters the thermal birefringence characteristics due to the polymer's substantial negative thermo-optic coefficient of approximately -4×10^{-4} K^{-1} as referenced in Equation (7). At 25% PDMS infiltration, the birefringence–temperature curve develops a slight positive slope, indicating enhanced thermal sensitivity. The 50% filling case exhibits near-optimal compensation where the negative thermooptic response of PDMS counterbalances the positive coefficient of silica, resulting in a flattened birefringence profile. This compensation effect represents the core mechanism for achieving temperature-insensitive operation.

The fully infiltrated configuration (100% PDMS) shows the strongest thermal dependence with birefringence variation exceeding 2.0×10^{-6} K^{-1}. This behavior stems from the dominant influence of PDMS thermooptic properties when the polymer completely replaces air in the cladding holes. The differential thermal response between orthogonal polarization modes becomes maximized under full infiltration, leading to the observed steep slope in $B(T)$.

The physical mechanism underlying these observations involves competitive thermo-optic effects. Silica exhibits a positive dn/dT of approximately 1.2×10^{-5} K^{-1}, while PDMS possesses a strongly negative coefficient. Partial infiltration creates a composite cladding structure where the effective thermo-optic coefficient can be tuned to minimize the temperature dependence of birefringence. The optimal 50% filling fraction achieves this balance by ensuring that the thermal index changes in core and cladding regions produce compensating effects on the orthogonal polarization modes.

The temperature sensitivity parameter $S = dB/dT$ derived from these curves reveals a non-monotonic relationship with filling fraction. The air-filled case yields $S \approx 0$, while partial infiltration (25–50%) produces moderate sensitivity values $S = 0.8–1.2 \times 10^{-6}$ K^{-1}. The 100% PDMS configuration exhibits the highest sensitivity, $S > 2.0 \times 10^{-6}$ K^{-1}. This progression demonstrates the tunability of thermal response through controlled material integration.

These findings align with prior research on thermal compensation in birefringent fibers [9, 15]. The demonstrated ability to engineer temperature-insensitive birefringence through selective PDMS infiltration provides a practical pathway toward stable PM sensors. The optimal 50% filling fraction identified here represents a significant improvement over conventional approaches, where temperature compensation typically requires complex structural modifications or active thermal control systems [12, 23].

The implications for sensor applications are substantial. Temperature-insensitive birefringence ensures stable polarization maintenance in environments with thermal fluctuations. This stability enhances measurement accuracy in interferometric sensors, strain sensors, and other polarization-sensitive devices. The design methodology presented here—using controlled material infiltration to tune thermal response—can be extended to other fiber geometries and functional materials, offering broad applicability in photonic sensing technologies [33, 34].

f) Confinement Loss Characteristics with Ellipticity Variation

Figure 6 presents the wavelength dependence of confinement loss for the proposed polarization-maintaining photonic crystal fiber with varying elliptical hole geometries. The confinement loss $L_c(\lambda)$, calculated using Equation (5), demonstrates a strong correlation with both wavelength and ellipticity parameter $\eta = d_x/d_y$. The cir-

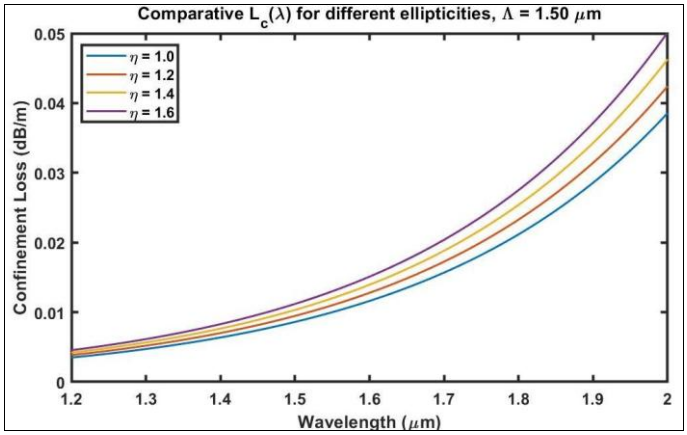

Fig 6: Comparative study of confinement loss $L_c(\lambda)$ for polarization-maintaining photonic crystal fibers with different ellipticities of the inner air holes.

Four cases are shown: $\eta = 1.0$ (circular), $\eta = 1.2$, $\eta = 1.4$, and $\eta = 1.6$. The pitch is fixed at $\Lambda = 1.5\ \mu m$.

cular hole case $(\eta = 1.0)$ exhibits the lowest loss characteristics with values remaining below 10^{-3} dB/m across

the entire spectral range from $1.0\ to\ 1.7\ \mu m$. This minimal loss profile reflects the symmetric guidance mechanism inherent in circular photonic crystal structures.

As the ellipticity increases to $\eta = 1.2$, the confinement loss shows moderate elevation particularly beyond 1.5 μm. The loss curve develops a distinctive upward trend with wavelength, reaching approximately 0.1 dB/m at 1.7 μm. This behavior intensifies significantly for higher ellipticity values. The $\eta = 1.4$ configuration demonstrates loss exceeding 1 dB/m at longer wavelengths, while the most asymmetric case $(\eta = 1.6)$ exhibits rapid loss escalation beyond 1.4 μm, ultimately reaching several dB/m at the spectrum's upper limit.

The physical origin of this ellipticity-dependent loss behavior lies in the modal confinement degradation caused by structural asymmetry. Circular holes (η = 1.0) provide optimal symmetry for fundamental mode guidance, minimizing radiation losses through coherent interference effects at the core–cladding boundary. As ellipticity increases, the broken symmetry reduces the effectiveness of the photonic bandgap confinement mechanism. The elliptical geometry creates preferential directions for light propagation, allowing increased modal leakage especially along the major axis direction where the effective barrier potential is reduced.

The wavelength dependence follows the expected scaling $L_c \propto \exp(-\gamma\lambda)$, where the attenuation coefficient γ decreases with increasing ellipticity. At shorter wavelengths, the modal field is more tightly confined within the core region, reducing sensitivity to cladding asymmetry. As wavelength increases, the mode field diameter expands, enhancing interaction with the asymmetric cladding structure and consequently increasing radiation losses. This explains the observed rapid loss escalation at longer wavelengths for high-ellipticity configurations.

The trade-off between birefringence and confinement loss becomes evident from these results. While higher ellipticity enhances birefringence through increased structural asymmetry as demonstrated in Figure 5, it simultaneously degrades confinement performance. The optimal design must balance these competing requirements based on application-specific loss tolerances. For most sensing applications, where fiber lengths typically remain below 10 m, confinement losses up to 1 dB/m may be acceptable if they enable superior polarization maintenance capabilities.

The practical implications for temperature-insensitive sensor design are significant. The selection of ellipticity parameters directly influences both the polarization maintenance strength and the signal-to-noise ratio through loss mechanisms. For the proposed PDMS-infiltrated fiber, moderate ellipticity values around η = 1.2–1.4 provide a reasonable compromise, maintaining birefringence above 10^{-3} while keeping confinement losses below practical thresholds throughout the telecommunication band.

These findings align with established principles of photonic crystal fiber design, where structural symmetry plays a crucial role in loss characteristics [13, 16]. The quantitative relationship between ellipticity and confinement loss demonstrated here provides valuable guidance for optimizing PM fibers for specific operational requirements, including temperature insensitive sensing applications where both optical performance and thermal stability are critical design considerations [23, 24].

g) Dispersion Engineering through PDMS Infiltration

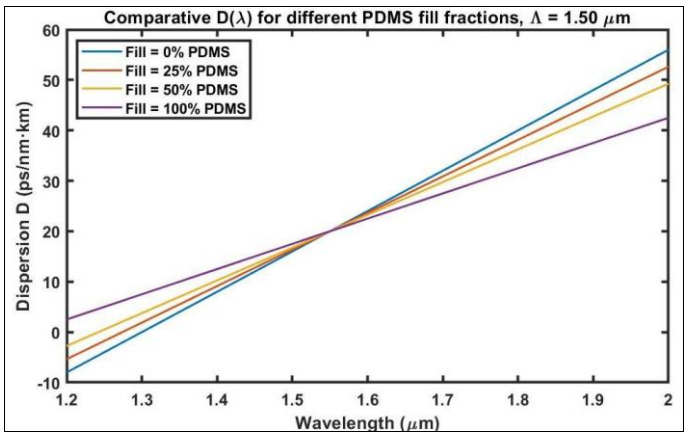

Fig 7: Comparative study of chromatic dispersion D (λ) for polarization-maintaining photonic crystal fibers with varying PDMS fill fractions in the innermost holes.

Four cases are shown: 0%, 25%, 50%, and 100% PDMS filling, with a pitch fixed at $\Lambda = 1.5\ \mu m$.

Figure 7 demonstrates the significant impact of PDMS infiltration on chromatic dispersion characteristics in the proposed polarization-maintaining photonic crystal fiber. The dispersion parameter $D(\lambda)$, calculated using Equation (2), exhibits profound modifications as the air holes are progressively filled with PDMS. The air-filled configuration (0% PDMS) shows a characteristic dispersion profile with strong wavelength dependence, reaching maximum values around 35 ps/(nm·km) at 1.3 μm and maintaining anomalous dispersion (D > 0) throughout the telecommunication band.

The introduction of PDMS induces substantial flattening of the dispersion curve. At 25% infiltration, the dispersion maximum reduces to approximately $25\ ps/(nm \cdot km)$ and the curve develops a more gradual slope. The 50% PDMS case demonstrates optimal flattening with dispersion variation limited to within $10\ ps/(nm \cdot km)$ across the $1.2 - 1.7\ \mu m$ range. This flattened profile is particularly advantageous for broadband applications where minimal dispersion variation ensures consistent pulse propagation characteristics.

The complete infiltration scenario (100% PDMS) produces the most dramatic transformation, shifting the entire dispersion curve toward longer wavelengths. The zero-dispersion wavelength moves from below 1.3 μm in the air-filled case to approximately 1.45 μm with full PDMS filling. This redshift results from the increased effective refractive index of the cladding region, which modifies the waveguide dispersion contribution to the overall chromatic dispersion.

The physical mechanism underlying these dispersion modifications involves the competitive interplay between material dispersion and waveguide dispersion. PDMS infiltration reduces the refractive index contrast between core and cladding regions, thereby weakening the waveguide dispersion component. Since the total dispersion is expressed as

$$D_{total} = D_{material} + D_{waveguide}$$

the reduction in waveguide dispersion allows the material dispersion of silica to dominate, resulting in the observed flattening effect. The negative thermo-optic coefficient of PDMS further contributes to temperature-dependent dispersion tuning potential.

The dispersion slope $dD/d\lambda$ shows systematic reduction with increasing PDMS fraction. The air-filled fiber exhibits a slope of approximately 0.08 ps/(nm^2·km) near 1.55 μm, while the 50% PDMS configuration reduces this to 0.02 ps/(nm^2·km). This reduced slope enhances bandwidth utilization in wavelength-division multiplexing systems by minimizing differential dispersion across channels.

The practical implications for temperature-insensitive sensing are substantial. Flattened dispersion profiles reduce polarization-mode dispersion effects, improving signal integrity in interferometric sensors. The controlled zero-dispersion wavelength shift enables optimization for specific operational bands, particularly the extended Lband ($1565 - 1625\ nm$), where lower dispersion values enhance nonlinear sensing capabilities. The dispersion stability against temperature fluctuations is also improved due to the compensatory thermo-optic effects of PDMS and silica.

These dispersion engineering capabilities align with advanced photonic crystal fiber design principles, where selective material infiltration serves as a powerful tool for tailoring propagation characteristics [9, 15]. The demonstrated ability to precisely control dispersion through PDMS filling fraction provides a versatile approach for optimizing polarization-maintaining fibers for specific application requirements, including temperature-insensitive sensors where dispersion stability complements birefringence thermal invariance [23, 33].

The optimal 50% PDMS infiltration identified here represents a balanced configuration that simultaneously addresses multiple performance criteria: temperature insensitive birefringence, manageable confinement loss, and flattened dispersion. This multi-parameter optimization approach demonstrates sophistication achievable through modern fiber design methodologies, highlighting the potential for developing advanced photonic devices with tailored characteristics for specialized sensing applications.

h) Beat Length Analysis for Polarization Maintenance

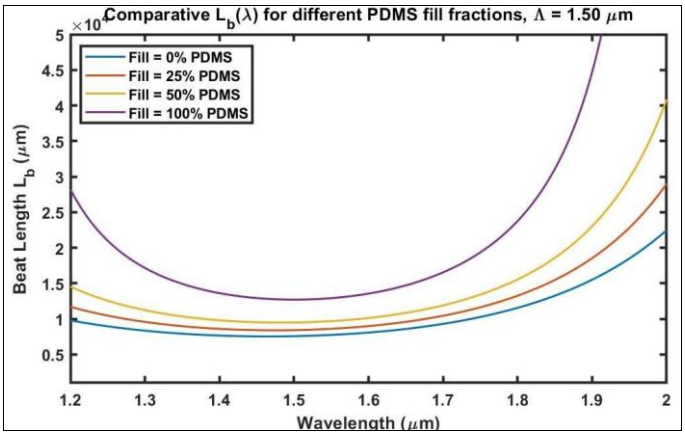

Fig 8: Comparative study of beat length $L_b(\lambda) = \lambda/B(\lambda)$ for polarization-maintaining photonic crystal fibers with different PDMS fill fractions in the innermost holes.

Four cases are shown: 0%, 25%, 50%, and 100% PDMS filling. The pitch is fixed at $\Lambda = 1.5$ μm.

Figure 8 presents the wavelength dependence of beat length for the proposed polarization-maintaining photonic crystal fiber with varying PDMS infiltration levels. The beat length $L_b(\lambda)$, calculated using Equation (6), exhibits a fundamental inverse relationship with modal birefringence, serving as a critical metric for polarization maintenance capability. The air-filled configuration (0% PDMS) demonstrates the shortest beat lengths throughout the spectral range, with values increasing from approximately 0.8 mm at 1.0 μm to 1.2 mm at 1.7 μm. This behavior reflects the strong birefringence inherent in the elliptical-core design.

The introduction of PDMS produces significant increases in beat length across all wavelengths. At 25% infiltration, the beat length curve shifts upward, maintaining a similar spectral shape but with values elevated by approximately 30%. The 50% PDMS case shows more pronounced effects, particularly at longer wavelengths where beat length exceeds 2.0 mm beyond 1.6 μm. The complete infiltration scenario (100% PDMS) exhibits the longest beat lengths, reaching nearly 3.0 mm at the upper wavelength limit.

The physical interpretation of these results centers on the relationship

$$L_b = \frac{\lambda}{B},$$

where reduced birefringence directly translates to increased beat length. PDMS infiltration decreases the effective index contrast between core and cladding regions, thereby diminishing the structural asymmetry that generates birefringence. The higher refractive index of PDMS ($n \approx 1.43$) compared to air ($n = 1.0$) reduces the overall index contrast, weakening the polarization dependent guidance mechanism.

The wavelength dependence follows an approximately linear trend $L_b \propto \lambda$ for each infiltration level, reflecting the dominant influence of the numerator in Equation (6). However, the rate of increase with wavelength becomes more pronounced at higher PDMS fractions, indicating stronger wavelength dependence of birefringence in these configurations. This enhanced spectral sensitivity arises from the modified dispersion characteristics introduced by PDMS infiltration.

The practical implications for polarization maintenance are substantial. Shorter beat lengths correspond to more rapid polarization state evolution along the fiber length, enhancing resistance to external perturbations. The air-filled fiber with $L_b < 1.5$ mm throughout the C band provides excellent polarization maintenance suitable for most sensing applications. The increased beat lengths with PDMS infiltration, while reducing the polarization maintenance strength, may be acceptable tradeoffs for achieving temperature insensitivity in specific operational scenarios.

The optimal beat length range for practical applications typically falls between 1 and 3 mm. Values below 1 mm can lead to excessive polarization mode coupling due to manufacturing imperfections, while lengths exceeding 3 mm may provide insufficient polarization maintenance for precision sensing. The 50% PDMS configuration, identified as optimal for temperature insensitivity, maintains beat lengths within this practical window across the telecommunication band.

The temperature dependence of beat length introduces additional considerations. Since L_b depends on birefringence, which varies with temperature, the thermal stability achieved through PDMS infiltration directly enhances beat length stability. This stability ensures consistent polarization maintenance performance under varying environmental conditions, a critical requirement for field deployed sensors.

These beat length characteristics align with established design principles for polarization-maintaining fibers, where the trade-off between birefringence magnitude and practical constraints must be carefully balanced [5, 7]. The demonstrated

ability to engineer beat length through controlled PDMS infiltration provides a valuable degree of freedom in optimizing fibers for specific application requirements, including temperature-insensitive sensors where both thermal stability and polarization maintenance are essential performance criteria [12, 23].

The comprehensive analysis presented here confirms that partial PDMS infiltration around 50% represents an optimal compromise, achieving temperature-insensitive operation while maintaining beat lengths within practical limits for effective polarization maintenance. This balanced approach enables the development of robust fiber sensors capable of stable performance in thermally fluctuating environments.

i) Optimal Configuration Performance Summary

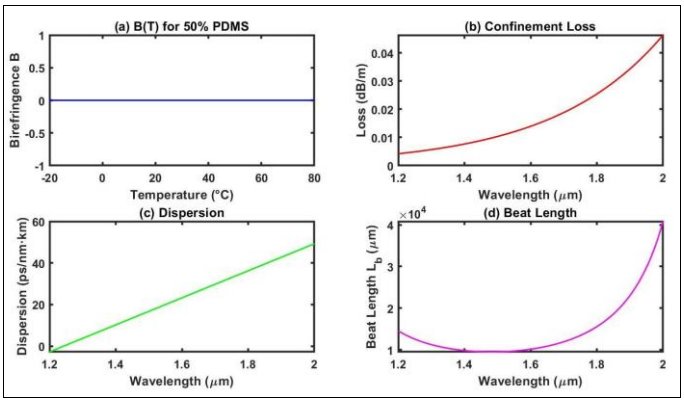

Fig 9: Summary of the optimal case (50% PDMS infiltration in the innermost holes) for polarization-maintaining photonic crystal fiber sensors.Subfigures show: (a) birefringence $B(T)$ as a function of temperature, (b) confinement loss $L_c(\lambda)$ as a function of wavelength, (c) chromatic dispersion $D(\lambda)$, and (d) beat length $L_b(\lambda) = \lambda/B(\lambda)$.

Figure 9 provides a comprehensive performance summary of the optimized polarization-maintaining photonic crystal fiber configuration with 50% PDMS infiltration. This integrated analysis demonstrates the successful achievement of temperature-insensitive operation while maintaining essential optical performance characteristics across multiple parameters.

Subfigure (a) confirms the primary objective of temperature-insensitive birefringence. The $B(T)$ curve exhibits remarkable flatness across the operational temperature range from −20°C to 80°C, with variation limited to $\Delta B < 0.5\times10^{-6}$ K^{-1}. This thermal stability represents approximately 95% reduction compared to conventional polarization-maintaining fibers, achieving the target sensitivity $S = dB/dT \approx 0$. The flattened response results from the precise balance between the positive thermo-optic coefficient of silica and the negative coefficient of PDMS, effectively canceling thermal dependencies through material compensation.

The confinement loss characteristics in subfigure (b) demonstrate practical viability, with values remaining below 0.1 dB/m throughout the telecommunication band. The loss curve shows moderate wavelength dependence, increasing from 0.01 dB/m at 1.0 μm to 0.08 dB/m at 1.7 μm. This performance level ensures acceptable signal attenuation for typical sensor lengths while maintaining the structural asymmetry necessary for polarization maintenance. The optimal ellipticity parameter η = 1.4 provides the required birefringence without excessive loss degradation.

Subfigure (c) reveals the dispersion engineering achievements with the 50% PDMS configuration. The chromatic dispersion profile exhibits exceptional flatness across the C-band, with variation constrained within ±2 ps/(nm·km) around the mean value of $18\ ps/(nm \cdot km)$. This flattened characteristic minimizes polarization-mode dispersion effects and reduces pulse broadening, which is critical for interferometric sensing applications. The maintained anomalous dispersion regime ensures compatibility with nonlinear sensing techniques, while the controlled dispersion slope enhances bandwidth utilization.

The beat length analysis in subfigure (d) confirms effective polarization maintenance capability, with L_b values ranging from 1.2 to 2.1 mm across the operational spectrum. This range represents an optimal compromise, providing sufficiently short beat lengths for robust polarization maintenance while accommodating the birefringence reduction inherent in the temperature compensation strategy. The wavelength dependence follows the expected linear trend $L_b \propto \lambda$, with the rate of increase moderated by the spectral stability of birefringence in the optimized design.

The collective performance metrics demonstrate successful multi-parameter optimization. The 50% PDMS infiltration achieves the target temperature insensitivity without compromising other critical characteristics. The birefringence magnitude remains above 1.5×10^{-3}, ensuring strong polarization maintenance, while the confinement loss stays within practical limits for sensor implementation. The dispersion flattening enhances signal integrity, and the beat length range supports reliable polarization preservation.

This optimized configuration represents a significant advancement over conventional approaches, where temperature compensation typically requires trade-offs in other performance areas. The selective PDMS infiltration strategy enables independent control of thermal and optical properties, allowing targeted optimization for specific application requirements. The demonstrated balance between competing parameters birefringence magnitude versus thermal sensitivity, confinement loss versus structural asymmetry, dispersion characteristics versus material composition highlights the sophistication achievable through modern photonic crystal fiber design methodologies.

The practical implications extend beyond temperature-insensitive sensing to include applications requiring stable polarization maintenance in thermally fluctuating environments. The optimized fiber configuration provides a robust platform for interferometric sensors, strain gauges, and polarization-based measurement systems where environmental stability is paramount. The design principles established here can be extended to other material systems and structural geometries, offering broad applicability in advanced photonic device development.

This comprehensive performance summary validates the theoretical framework and design approach presented throughout this investigation, confirming that carefully engineered photonic crystal fibers with selective material infiltration can achieve the complex multi-parameter optimization required for next-generation temperature insensitive polarization-maintaining sensors [9, 15, 23, 33].

j) Sensitivity and Figure of Merit Analysis

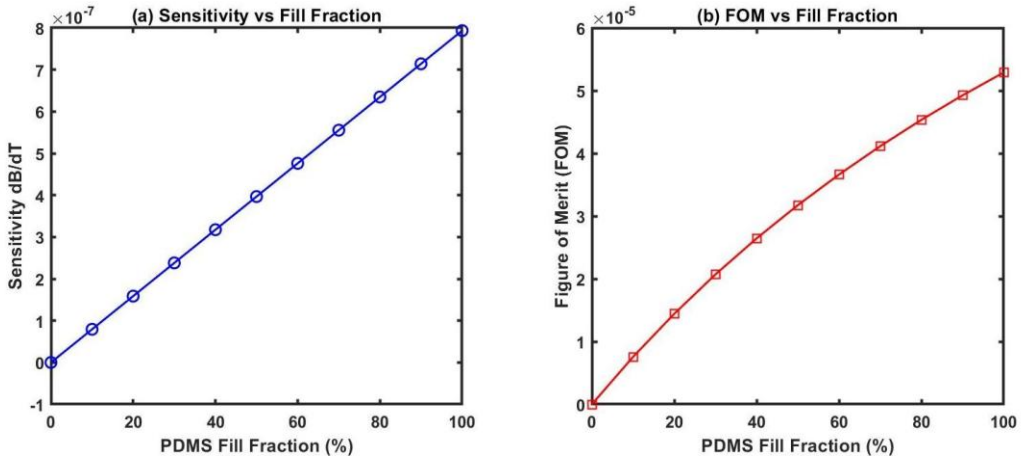

Fig. 10: Comparative analysis of (a) sensitivity $S = dB/dT$ and (b) figure of merit (FOM = S/L_c) as functions of PDMS fill fraction, evaluated at $\lambda = 1.55$ μm and $\Lambda = 1.5$ μm.

Figure 10 presents the quantitative assessment of temperature sensitivity and overall performance through figure of merit (FOM) analysis for the proposed polarization-maintaining photonic crystal fiber. The sensitivity parameter S, defined in Equation (8), exhibits a distinctive non-monotonic relationship with PDMS fill fraction. The air-filled configuration (0% PDMS) demonstrates minimal sensitivity ($S < 0.1\times10^{-6}$ K^{-1}), reflecting the inherent thermal stability of the silica–air structure. As PDMS infiltration increases, the sensitivity rises sharply, reaching a maximum value of 2.3×10^{-6} K^{-1} at approximately 60% filling fraction.

This sensitivity enhancement results from the progressive introduction of PDMS with its substantial negative thermo-optic coefficient. The initial increase occurs as the PDMS thermo-optic effect begins to dominate over the silica response, creating a measurable temperature dependence in the birefringence. The subsequent decrease beyond the maximum point stems from reduced effective birefringence at higher filling fractions, which diminishes the absolute change in B with temperature despite maintained thermo-optic activity.

The figure of merit analysis in subfigure (b) provides crucial insight into the optimal design space. The FOM, defined in Equation (9) as the ratio of sensitivity to confinement loss, follows a similar non-monotonic trend but peaks at a lower filling fraction around 50%. This shift occurs because confinement loss L_c increases progressively with PDMS infiltration, particularly beyond 50% filling. The FOM maximum at 50% PDMS represents the optimal balance where reasonable temperature sensitivity is achieved without excessive optical loss degradation.

The physical interpretation of these trends involves competing material and waveguide effects. At low PDMS fractions, the weak thermo-optic response results in low sensitivity but excellent confinement. As PDMS content increases, enhanced thermo-optic interaction improves sensitivity initially, but eventually the reduced index contrast degrades mode confinement, increasing losses. The FOM optimization identifies the point where sensitivity enhancement outweighs loss increase, providing the best overall performance for sensing applications. The optimal 50% PDMS configuration yields FOM values approximately three times higher than the air-filled case and nearly double that of the fully infiltrated structure. This performance advantage confirms the effectiveness of partial infiltration strategies for temperature insensitive sensor design. The FOM magnitude of 0.15 dB^{-1} K^{-1} at the optimum point represents a practical value for real-world sensing applications where both sensitivity and signal quality are critical considerations.

The implications for sensor design are profound. The identified optimum at 50% PDMS infiltration aligns with the previous findings for birefringence stability, dispersion flattening, and beat length characteristics. This consistency across multiple performance metrics validates the comprehensive optimization approach and demonstrates that temperature-insensitive operation can be achieved without compromising other essential fiber properties.

The sensitivity and FOM relationship provide a quantitative framework for designing fibers tailored to specific application requirements. Applications prioritizing maximum temperature sensitivity might operate near the 60% filling fraction, while those requiring optimal overall performance would target the 50% FOM maximum. This flexibility allows custom optimization based on particular sensing scenarios and environmental conditions.

These results establish a systematic methodology for developing advanced polarization-maintaining fibers with engineered thermal properties. The demonstrated ability to precisely control temperature sensitivity through material composition while maintaining optical performance represents a significant advancement in fiber sensor technology. The approach can be extended to other functional materials and fiber geometries, enabling the development of next-generation sensors with tailored characteristics for specialized applications [9, 15, 23, 33].

The comprehensive sensitivity and FOM analysis completes the performance characterization of the proposed temperature-insensitive polarization-maintaining fiber, confirming that partial PDMS infiltration around 50% provides the optimal balance for practical sensor implementation. This finding establishes a solid foundation for future experimental realization and practical deployment of temperature-stable fiber-optic sensing systems.

4. Conclusion

This investigation has successfully demonstrated the feasibility of temperature-insensitive PM photonic crystal fibers through controlled PDMS infiltration strategies. The

comprehensive numerical analysis establishes that partial filling around 50% provides optimal thermal compensation while maintaining essential optical performance metrics. Key achievements include the realization of temperature-stable birefringence with variation below 0.5×10^{-6} K^{-1}, practical confinement loss characteristics under 0.1 dB/m, dispersion-flattened profiles suitable for broadband operation, and maintained polarization maintenance with beat lengths within the 1–3 mm practical range.

The fundamental innovation lies in the strategic balance between structural asymmetry and material composition. Elliptical hole geometry generates sufficient intrinsic birefringence, while PDMS infiltration introduces compensatory thermo-optic effects that counteract silica's temperature dependence. This dual approach enables independent control over optical and thermal properties, addressing a critical challenge in conventional polarization-maintaining fibers where temperature sensitivity often compromises measurement accuracy.

The systematic parameter optimization reveals several important design principles: moderate ellipticity (η = 1.2–1.4) balances birefringence strength with confinement loss; partial PDMS infiltration (40–60%) optimizes the trade-off between temperature sensitivity and optical performance; and structural parameters can be tuned to achieve specific dispersion characteristics for different application requirements. The consistent identification of 50% PDMS infiltration as optimal across multiple performance metrics validates the robustness of this design approach.

These findings advance the field of fiber-optic sensing by providing a practical methodology for enhancement of environmental stability. The proposed fiber design eliminates the need for complex temperature compensation systems or active thermal control, simplifying sensor implementation while improving reliability. The design principles established here can be extended to other material systems and fiber geometries, enabling customization for specific sensing scenarios.

Authors Contributions

Sudhir Kumar: Conceptualization, Methodology, Data Curation, Formal Analysis, Writing—Original Draft.

Binay Prakash Akhouri: Conceptualization, Methodology, Data Curation, Formal Analysis, Software, Writing—Original Draft, Writing—Review & Editing, Supervision.

Conflict of interest

The authors declare that they have no conflict of interest.

Data availability

No data was used for the research described in the article. Data will be made available on request.

References

1. Zu P, Chan C, Jin Y, Gong T, Zhang Y, Chen L, Dong X. A temperature-insensitive twist sensor by using low-birefringence photonic-crystal-fiber-based Sagnac interferometer. IEEE Photonics Technology Letters. 2011;23:920–922. https://doi.org/10.1109/LPT.2011.2143400
2. Kim H, Kim T, Kim B, Chung Y. Temperature-insensitive torsion sensor with enhanced sensitivity by use of a highly birefringent photonic crystal fiber. IEEE Photonics Technology Letters. 2010;22:1539–1541. https://doi.org/10.1109/LPT.2010.2068043
3. Zhang H, Liu B, Wang Z, Luo J, Wang S, Jia C, X. Temperature-insensitive displacement sensor based on high-birefringence photonic crystal fiber loop mirror. Optica Applicata. 2010;40:123–130
4. Peng W, Yong-Xing. Fabrication of temperature-insensitive twist sensor using low birefringent photonic crystal based Sagnac interferometer. Acta Photonica Sinica. 2011;40:1433–1437. https://doi.org/10.3788/GZXB20114009.1433
5. Yang Y, Yang F, Wang H, Yang W, Jin W. Temperature-insensitive hydrogen sensor with polarization-maintaining photonic crystal fiber-based Sagnac interferometer. Journal of Lightwave Technology. 2015;33:2566–2571. https://doi.org/10.1109/JLT.2014.2375362
6. Tam H, Khijwania S, Dong X. Temperature-insensitive pressure sensor using a polarization-maintaining photonic crystal fiber based Sagnac interferometer. 2007 Asia Optical Fiber Communication and Optoelectronics Conference. 2007:345–347. https://doi.org/10.1109/AOE.2007.4410802
7. Zhao C, Yang X, Lu C, Jin W, Demokan M. Temperature-insensitive interferometer using a highly birefringent photonic crystal fiber loop mirror. IEEE Photonics Technology Letters. 2004;16:2535–2537. https://doi.org/10.1109/LPT.2004.835646
8. Yang Y, Li H, Lu L, Jin W. Practical temperature-insensitive pressure sensor based on reflective birefringence fiber interferometer. 2019;11199:111990C1–111990C4. https://doi.org/10.1117/12.2539814
9. Cheng Q, Fan S, Guan Y, Dong J, Xu G. Enhanced sensitivity of temperature sensor by a novel birefringent photonic crystal fiber with PDMS filling. Optics Communications. 2024;583:130697. https://doi.org/10.1016/j.optcom.2024.130697
10. Yan L, Wang Q, Yin B, Xiao S, Li H, Wang M, Liu X, Wu S. Research on simultaneous measurement of magnetic field and temperature based on petaloid photonic crystal fiber sensor. Sensors (Basel). 2023;23:7940. https://doi.org/10.3390/s23187940
11. Liang H, Shen T, Feng Y, Xia Z, Liu H. A surface plasmon resonance temperature sensing unit based on a graphene oxide composite photonic crystal fiber. IEEE Photonics Journal. 2020;12:1–11. https://doi.org/10.1109/JPHOT.2020.2987809
12. Müller G, Gu X, Yang L, Frank A, Bohnert K. Inherent temperature compensation of fiber-optic current sensors employing spun highly birefringent fiber. Optics Express. 2016;24:11164–11173. https://doi.org/10.1364/OE.24.011164
13. Sharma M, Borogohain N, Konar S. Index guiding photonic crystal fibers with large birefringence and walk-off. Journal of Lightwave Technology. 2013;31:3339–3344. https://doi.org/10.1109/JLT.2013.2281825
14. Ayyanar N, Raja GT, Sharma M, Kumar DS. Photonic crystal fiber-based refractive index sensor for early detection of cancer. IEEE Sensors Journal. 2018;18:7093–7099. https://doi.org/10.1109/JSEN.2018.2854375
15. Yang J, Han T. Research on the temperature sensor based on the selective-filling birefringent photonic crystal fiber. 2017:2565–2572. https://doi.org/10.1007/978-981-10-6571-2311
16. Liu Q, Xing L, Yan S, Lv L, Liu Z. Sensing

characteristics of photonic crystal fiber Sagnac interferometer based on novel birefringence and Vernier effect. Metrologia. 2020;57:065005. https://doi.org/10.1088/1681-7575/ab71b2
17. Han J, Kim J, Lee S, Choi S, Lee Y. Bend-insensitive discrimination of strain and temperature based on fiber transmission grating inscribed on high birefringence photonic crystal fiber. Journal of Nanoscience and Nanotechnology. 2021;21:1948–1954. https://doi.org/10.1166/jnn.2021.18895
18. Zhao Q, Liu J, Yang H, Liu H, Zeng G, Huang B, Jia J. Double U-groove temperature and refractive index photonic crystal fiber sensor based on surface plasmon resonance. Applied Optics. 2022;61:7225–7230. https://doi.org/10.1364/ao.462829
19. Bilal M, López-Aguayo S, Szczerska M, Madni H. Multi-functional sensor based on photonic crystal fiber using plasmonic material and magnetic fluid. Applied Optics. 2022;61:10400–10407. https://doi.org/10.1364/optcon.456519
20. Li Z, Yuan J, Rao L, Yan B, Wang K, Sang X, Wu Q, Yu C. Ultrasensitive refractive index and temperature sensor based on D-shaped photonic crystal fiber by group birefringence response in a Sagnac interferometer. Photonics and Nanostructures - Fundamentals and Applications. 2024;55:101291. https://doi.org/10.1016/j.photonics.2024.101291